

This is a repository copy of *Comparison of independent evolutionary origins reveals both convergence and divergence in the metabolic mechanisms of symbiosis*.

White Rose Research Online URL for this paper:

<https://eprints.whiterose.ac.uk/id/eprint/153412/>

Version: Accepted Version

Article:

Sorenson, Megan E.S., Wood, Andrew James orcid.org/0000-0002-6119-852X, Minter, Ewan John Arrbuthnott et al. (3 more authors) (2020) Comparison of independent evolutionary origins reveals both convergence and divergence in the metabolic mechanisms of symbiosis. *Current Biology*. 328-334.E4. ISSN: 0960-9822

<https://doi.org/10.1016/j.cub.2019.11.053>

Reuse

This article is distributed under the terms of the Creative Commons Attribution-NonCommercial-NoDerivs (CC BY-NC-ND) licence. This licence only allows you to download this work and share it with others as long as you credit the authors, but you can't change the article in any way or use it commercially. More information and the full terms of the licence here: <https://creativecommons.org/licenses/>

Takedown

If you consider content in White Rose Research Online to be in breach of UK law, please notify us by emailing eprints@whiterose.ac.uk including the URL of the record and the reason for the withdrawal request.

Current Biology

Comparison of independent evolutionary origins reveals both convergence and divergence in the metabolic mechanisms of symbiosis

--Manuscript Draft--

Manuscript Number:	CURRENT-BIOLOGY-D-19-01502R2
Full Title:	Comparison of independent evolutionary origins reveals both convergence and divergence in the metabolic mechanisms of symbiosis
Article Type:	Report
Corresponding Author:	Michael Brockhurst University of Sheffield Sheffield, UNITED KINGDOM
First Author:	Megan Sorensen
Order of Authors:	Megan Sorensen Jamie Wood Ewan Minter Chris Lowe Duncan Cameron Michael Brockhurst
Abstract:	<p>Through the merger of once independent lineages, symbiosis promotes the acquisition of new traits and the exploitation of inaccessible ecological niches [1,2], driving evolutionary innovation and important ecosystem functions [3–6]. The transient nature of establishment makes study of symbiotic origins difficult, but experimental comparison of independent originations could reveal the degree of convergence in the underpinning mechanisms [7,8]. We compared the metabolic mechanisms of two independent origins of the <i>Paramecium bursaria</i>-<i>Chlorella</i> photosymbiosis [9–11] using a reciprocal metabolomic pulse-chase method. This showed convergent patterns of nutrient exchange and utilisation for host-derived nitrogen in the <i>Chlorella</i> genotypes [12,13] and symbiont-derived carbon in the <i>P. bursaria</i> genotypes [14,15]. Consistent with a convergent primary nutrient exchange, partner-switched host-symbiont pairings were functional. Direct competition of hosts containing native or recombined symbionts against isogenic symbiont-free hosts showed that the fitness benefits of symbiosis for hosts increased with irradiance but varied by genotype. Global metabolism varied more between the <i>Chlorella</i> than the <i>P. bursaria</i> genotypes, and suggested divergent mechanisms of light management. Specifically, the algal symbiont genotypes either produced photo-protective carotenoid pigments at high irradiance or more chlorophyll, resulting in corresponding differences in photosynthetic efficiency and non-photochemical quenching among host-symbiont pairings. These data suggest that the multiple origins of the <i>P. bursaria</i>-<i>Chlorella</i> symbiosis use a convergent nutrient exchange, whereas other photosynthetic traits linked to the functioning of the photosymbiosis have diverged. While convergence enables partner-switching among diverse strains, phenotypic mismatches resulting from divergence of secondary-symbiotic traits could mediate host-symbiont specificity in nature.</p>



The
University
Of
Sheffield.

THE DEPARTMENT OF ANIMAL AND PLANT SCIENCES
Alfred Denny Building, University of Sheffield, Sheffield, S10 2TN, UK

Professor Michael Brockhurst
Professor of Microbial Evolution
m.brockhurst@sheffield.ac.uk

12 November 19

Dear Dr. Anne Knowlton,

We are grateful for the opportunity to revise our manuscript. We have made all requested editorial changes and completed the tasks in the final checklist.

We hope that our manuscript is now acceptable for publication.

Yours sincerely,

A handwritten signature in blue ink, appearing to be 'M. Brockhurst'.

Prof. Michael Brockhurst (on behalf of the authors)

We are pleased that the reviewers are completely satisfied with the revisions. We have made all requested editorial changes, most significantly reducing the total number of figures to four by combining Figures 3 and 4 into the new Figure 3.

CELL PRESS DECLARATION OF INTERESTS POLICY

Transparency is essential for a reader's trust in the scientific process and for the credibility of published articles. At Cell Press, we feel that disclosure of competing interests is a critical aspect of transparency. Therefore, we ask that all authors disclose any financial or other interests related to the submitted work that (1) could affect or have the perception of affecting the author's objectivity, or (2) could influence or have the perception of influencing the content of the article, in a "Declaration of Interests" section.

What types of articles does this apply to?

We ask that you disclose competing interests for all submitted content, including research articles as well as front matter (e.g., Reviews, Previews, etc.) by completing and submitting the "Declaration of Interests" form below. We also ask that you include a "Declaration of Interests" section in the text of all research articles even if there are no interests declared. For front matter, we ask you to include a "Declaration of Interests" section only when you have information to declare.

What should I disclose?

We ask that you and all authors disclose any personal financial interests (examples include stocks or shares in companies with interests related to the submitted work or consulting fees from companies that could have interests related to the work), professional affiliations, advisory positions, board memberships, or patent holdings that are related to the subject matter of the contribution. As a guideline, you need to declare an interest for (1) any affiliation associated with a payment or financial benefit exceeding \$10,000 p.a. or 5% ownership of a company or (2) research funding by a company with related interests. You do not need to disclose diversified mutual funds, 401ks, or investment trusts.

Where do I declare competing interests?

Competing interests should be disclosed on the "Declaration of Interests" form as well as in the last section of the manuscript before the "References" section, under the heading "Declaration of Interests". This section should include financial or other competing interests as well as affiliations that are not included in the author list. Examples of "Declaration of Interests" language include:

"AUTHOR is an employee and shareholder of COMPANY."

"AUTHOR is a founder of COMPANY and a member of its scientific advisory board."

NOTE: Primary affiliations should be included on the title page of the manuscript with the author list and do not need to be included in the "Declaration of Interests" section. Funding sources should be included in the "Acknowledgments" section and also do not need to be included in the "Declaration of Interests" section. (A small number of front-matter article types do not include an "Acknowledgments" section. For these articles, reporting of funding sources is not required.)

What if there are no competing interests to declare?

For *research* articles, if you have no competing interests to declare, please note that in a "Declaration of Interests" section with the following wording:

"The authors declare no competing interests."

Front-matter articles do not need to include this section when there are no competing interests to declare.

CELL PRESS DECLARATION OF INTERESTS FORM

If submitting materials via Editorial Manager, please complete this form and upload with your final submission. Otherwise, please e-mail as an attachment to the editor handling your manuscript.

Please complete each section of the form and insert any necessary “Declaration of Interest” statement in the text box at the end of the form. A matching statement should be included in a “Declaration of Interest” section in the manuscript.

Institutional Affiliations

We ask that you list the current institutional affiliations of all authors, including academic, corporate, and industrial, on the title page of the manuscript. ***Please select one of the following:***

- ☒ All affiliations are listed on the title page of the manuscript.
- ☐ I or other authors have additional affiliations that we have noted in the “Declaration of Interests” section of the manuscript and on this form below.

Funding Sources

We ask that you disclose all funding sources for the research described in this work. ***Please confirm the following:***

- ☒ All funding sources for this study are listed in the “Acknowledgments” section of the manuscript.*

*A small number of front-matter article types do not include an “Acknowledgments” section. For these, reporting funding sources is not required.

Competing Financial Interests

We ask that authors disclose any financial interests, including financial holdings, professional affiliations, advisory positions, board memberships, receipt of consulting fees etc., that:

- (1) could affect or have the perception of affecting the author’s objectivity, *or*
- (2) could influence or have the perception of influencing the content of the article.

Please select one of the following:

- ☒ The authors have no financial interests to declare.
- ☐ I or other authors have noted any financial interests in the “Declaration of Interests” section of the manuscript and on this form below.

Advisory/Management and Consulting Positions

We ask that authors disclose any position, be it a member of a Board or Advisory Committee or a paid consultant, that they have been involved with that is related to this study. ***Please select one of the following:***

- ☒ The authors have no positions to declare.
- ☐ I or other authors have management/advisory or consulting relationships noted in the “Declaration of Interests” section of the manuscript and on this form below.

Patents

We ask that you disclose any patents related to this work by any of the authors or their institutions. ***Please select one of the following:***

- ☒ The authors have no related patents to declare.
- ☐ I or one of my authors have a patent related to this work, which is noted in the “Declaration of Interests” section of the manuscript and on this form below.

Please insert any “Declaration of Interests” statement in this space. This exact text should also be included in the “Declaration of Interests” section of the manuscript. If no authors have a competing interest, please insert the text, “The authors declare no competing interests.”

The authors declare no conflicting interests

On behalf of all authors, I declare that I have disclosed all competing interests related to this work. If any exist, they have been included in the “Declaration of Interests” section of the manuscript.

Name:

Michael Brockhurst

**Manuscript
Number (if
available):**

CURRENT-BIOLOGY-D-19-01502R1

Comparison of independent evolutionary origins reveals both convergence and divergence in the metabolic mechanisms of symbiosis

Megan E. S. Sørensen¹, A. Jamie Wood², Ewan J. A. Minter¹, Chris D. Lowe³,
Duncan D. Cameron¹, Michael A. Brockhurst¹

1. Department of Animal and Plant Sciences, University of Sheffield, Sheffield S10
2TN, UK

2. Department of Biology, University of York, York YO10 5DD, UK

3. Centre for Ecology and Conservation, University of Exeter, Penryn Campus,
Cornwall TR10 9FE, UK

Lead contact Michael Brockhurst (m.brockhurst@sheffield.ac.uk)

Summary

Through the merger of once independent lineages, symbiosis promotes the acquisition of new traits and the exploitation of inaccessible ecological niches [1,2], driving evolutionary innovation and important ecosystem functions [3–6]. The transient nature of establishment makes study of symbiotic origins difficult, but experimental comparison of independent originations could reveal the degree of convergence in the underpinning mechanisms [7,8]. We compared the metabolic mechanisms of two independent origins of the *Paramecium bursaria-Chlorella* photosymbiosis [9–11] using a reciprocal metabolomic pulse-chase method. This showed convergent patterns of nutrient exchange and utilisation for host-derived nitrogen in the *Chlorella* genotypes [12,13] and symbiont-derived carbon in the *P. bursaria* genotypes [14,15]. Consistent with a convergent primary nutrient exchange, partner-switched host-symbiont pairings were functional. Direct competition of hosts containing native or recombined symbionts against isogenic symbiont-free hosts showed that the fitness benefits of symbiosis for hosts increased with irradiance but varied by genotype. Global metabolism varied more between the *Chlorella* than the *P. bursaria* genotypes, and suggested divergent mechanisms of light management. Specifically, the algal symbiont genotypes either produced photo-protective carotenoid pigments at high irradiance or more chlorophyll, resulting in corresponding differences in photosynthetic efficiency and non-photochemical quenching among host-symbiont pairings. These data suggest that the multiple origins of the *P. bursaria-Chlorella* symbiosis use a convergent nutrient exchange, whereas other photosynthetic traits linked to the functioning of the photosymbiosis have diverged. While convergence enables partner-switching among diverse strains,

phenotypic mismatches resulting from divergence of secondary-symbiotic traits could mediate host-symbiont specificity in nature.

Results and Discussion

Independent evolutionary origins of a beneficial symbiotic relationship suggests that a strong selective advantage has, on multiple occasions, overcome the inherent conflict between the self-interest of the partners [16,17]. Independent origins of symbiosis appear to be common and have been reported in diverse symbiotic relationships [18–21]. Experimental comparison of independent origins could reveal the degree of convergence versus divergence in the underpinning mechanisms [7,8]. A convergent nutrient exchange would suggest evolutionary constraint and limited viable routes to symbiosis, but may allow partner-switching between independent lineages, whereas divergence would tend to drive host-symbiont specificity. Here we use the experimentally tractable microbial symbiosis between the heterotrophic ciliate *Paramecium bursaria* and the photosynthetic green alga *Chlorella* sp [9]. These species engage in a facultative photosymbiosis that is widely distributed in freshwater habitats [22], wherein ~100-600 algal cells live inside a ciliate cell and provide products of photosynthesis in exchange for organic nitrogen [14,23]. This symbiotic interaction has originated multiple times and forms two distinct biogeographical clades, specifically, the European clade and the American/Japanese clade [10,11]. Using a representative of each clade [the strain 186b originally isolated in the UK and strain HA1 originally isolated in Japan (Table S1); clade identity was confirmed by diagnostic PCR (Figure S1)] we first tested whether these strains used convergent biochemical mechanisms of carbon (from the photosynthetic endosymbiotic *Chlorella*) for nitrogen (acquired by the protist host through the

ingestion and digestion of free-living bacteria) exchange [14]. To do this, we devised a reciprocal, temporally-resolved, metabolomic pulse chase experiment that simultaneously monitored nitrogen and carbon assimilation in the symbiont and host, respectively. Specifically, using ^{15}N -labelled bacterial necromass, we traced isotopic enrichment derived from N assimilated through *P. bursaria* digestion in *Chlorella* metabolites. In parallel, using ^{13}C -labelled HCO_3^- we traced isotopic enrichment derived from C fixed by *Chlorella* photosynthesis in *P. bursaria* metabolites. The quantity of every individual metabolite in each sample was determined using Liquid Chromatography Time of Flight Mass Spectrometry (LC-ToFMS). This allowed the metabolic fate of resources exchanged between symbiotic partners to be quantified over time, allowing comparison of symbiotic metabolism between the strains.

We used Random Forest models, a form of computational learning involving the construction of an extensive array of possible compatible decision trees, to identify which metabolites were associated with isotopic enrichment. Among *Chlorella* metabolites we observed a shared ^{15}N isotopic enrichment response among strains (i.e. high-ranking score in both strains) in 46% of all metabolites (78 % of nitrogen-containing metabolites), suggesting that both *Chlorella* strains directed the exchanged nitrogen through metabolism in similar ways (Figure 1). Similarly, we observed a shared ^{13}C enrichment response in 75 % of *P. bursaria* metabolites (78% of carbon-containing metabolites), suggesting a high degree of convergence between the *P. bursaria* host strains in how they utilised the C derived from their algal symbionts (Figure 1). The pattern of shared enrichment among strains was consistently high for both ^{15}N and ^{13}C isotopic enrichment across all sampled time-points, suggesting a conserved nutrient exchange (Figure 1). Smaller proportions of

metabolites showed an asymmetric response (i.e., were high-ranked in one strain but low-ranked in the other; for ^{15}N enrichment, 20.55% in 186b *Chlorella* and 9.55% in HA1 *Chlorella*; for ^{13}C enrichment 13.17% in 186b *P. bursaria* and 3.42% in HA1 *P. bursaria*), suggesting only limited divergence in utilisation of exchanged metabolites has occurred between these host-symbiont clades.

Co-enriched metabolites with the strongest enrichment over time were identified using LC-ToFMS (simultaneously resolving the monoisotopic mass and chromatographic retention time for each M/Z). For ^{15}N co-enrichment in *Chlorella* (Table S2), we identified metabolites associated with the amino acid and purine pathways, which have both previously been suggested as probable N exchange metabolites in this symbiosis [12,24–27]. Targeted analyses of these pathways were used to calculate the enrichment dynamics in the constituent metabolites. These dynamics indicated that an amino acid is the more likely N exchange metabolite from *P. bursaria* to *Chlorella* in both clades. Although our first sampling time-point was not early enough to permit direct observation of metabolite exchange itself, downstream enrichment profiles suggest that the most likely candidate exchange metabolite is arginine (see Figure S4), an amino acid known to support growth of *Chlorella* as its sole N source [28]. In addition, we observed co-enrichment in larger, N-rich metabolites, including chlorophyll precursors, which most likely represent the largest N-sinks for *Chlorella*, thus becoming enriched in ^{15}N as a function of N demand. For ^{13}C enrichment in *P. bursaria* (Table S3), we identified metabolites involved in carbohydrate and lipid metabolism, suggesting that symbiont derived C was directed to carbon storage, as well as enrichment in central and amino acid metabolism, which are likely to have a high turnover of carbon and represent strong carbon sinks.

For some carbohydrate storage metabolites, we observed stronger differences in ^{13}C enrichment between light conditions in the 186b compared to the HA1 strain (Figure S3), indicating strain differences in the rate of flux through some of co-enriched pathways.

The pulse-chase analysis suggests that these *P. bursaria-Chlorella* strains, representing independent origins of the symbiosis, show convergent utilisation of partner-derived nutrients, and we hypothesised therefore that partner-switched host-symbiont pairings would be functional. To test this, we performed a reciprocal cross-infection experiment whereby the *P. bursaria* host strains were cured of their native algal symbiont, and subsequently re-infected with either their native algal symbiont or the reciprocal non-native algal symbiont. We then directly competed each host-symbiont pairing against its respective symbiont-free host strain across a light gradient. Note that reinfection of aposymbiotic host populations by symbionts occurs over far longer timescales (i.e. several weeks) than the competition assay, such that this process is unlikely to affect relative fitness estimates. We used flow cytometry to quantify the proportion of green (with symbiont) versus white (symbiont-free) host cells at the start and end of the growth cycle to calculate the selection rate [23], thus providing a direct measure of the fitness effect of symbiosis for hosts. All the symbiont pairings showed a classic photosymbiotic reaction norm, such that the relative fitness of hosts with symbionts versus hosts without symbionts increased with increasing irradiance (Figure 2), and more steeply in the HA1 host background (host genotype by light environment interaction, ANOVA, $F_{3,31} = 29.34$, $P < 0.001$). This confirms that both host genotypes could derive the benefits of symbiosis from

either of the symbiont genotypes, but that the fitness effect of symbiosis varied between strains.

These light-dependent differences in the fitness of the host-symbiont pairings suggest that the HA1 and 186b strains may have diverged in aspects of their metabolism and physiology besides the primary symbiotic nutrient exchange. To characterise potential differences in global metabolism between the HA1 and 186b host-symbiont strains, we performed untargeted metabolomics analyses on the unlabelled metabolites from the separated *Chlorella* and *P. bursaria* fractions of both the native host-symbiont pairings. We observed a range of metabolites that differentiated the 186b and HA1 *Chlorella* strains (Table S4), and metabolism differed more between strains than it did between light conditions within strains (Figure 3 panels A-D). Notably, the HA1 *Chlorella* strain displayed higher levels of several carotenoids than the 186b *Chlorella* strain, particularly at high irradiance, whereas the 186b *Chlorella* strain displayed higher levels of metabolites involved in chlorophyll and ubiquinol metabolism than the HA1 *Chlorella* strain at both low and high irradiance (Figure 3 panels E-J). Fewer metabolites distinguished the global metabolism of the *P. bursaria* strains (Table S4). In all cases these metabolites were present at higher levels in the 186b *P. bursaria* strain compared to the HA1 *P. bursaria* strain (Figure S2), and neither strain's metabolism varied significantly with irradiance (Figure S2). The identified metabolites that distinguished the strains were associated with a range of functions, including amino acid metabolism, amino sugars, and sphingolipid metabolism. Several other metabolites, although present in the host fraction, are likely to have been secreted into the host cytoplasm by the algal symbiont or be derived from the bacterial necromass. These include a zeatin

candidate, which may play a role in *Chlorella* signalling, and several metabolites identified as putative antibiotics.

The clear differences in global metabolism between the algal strains suggests that they may vary in their photophysiology. To test this, we measured several key photochemical parameters in the native and partner-switched host-symbiont pairings acclimated to a range of light levels. For two measures of photosynthetic efficiency — F_v/F_m (the intrinsic efficiency of photosystem II [PSII], Figure 4A) and Φ_{PSII} (the proportion of the light absorbed by chlorophyll associated with PSII that is used in photochemistry, Figure 4B) [29] — we observed a significant host genotype by symbiont genotype by light environment interaction [for F_vF_m ANOVA, $F_{7,232} = 86.41$, $P < 0.001$; for Φ_{PSII} nlme model intercept summary ANOVA, $F_{11,24} = 11.66$, $P < 0.001$ (see Data S1 for full statistical output)]. In the HA1 *P. bursaria* host, the pattern of photosynthetic efficiency across the light gradient did not vary with algal strain, whereas in the 186b *P. bursaria* host, the native 186b *Chlorella* showed lower photosynthetic efficiency than the HA1 *Chlorella* at low growth irradiance, but the pattern was reversed at high growth irradiance. These patterns are consistent with the observed differences in carotenoid metabolism among the *Chlorella* strains: The HA1 *Chlorella* produced more carotenoids at high irradiance than the 186b *Chlorella*; because carotenoids perform a role in photoprotection they can therefore decrease the light energy that reaches the photosystems thus limiting photosynthesis.

Non-photochemical quenching is used by photosynthetic organisms to safely deal with excess and potentially damaging light energy and was estimated using the normalised Stern-Volmer coefficient (NSV). The intercept of the NSV response

(Figure 4C) across the actinic light gradient was significantly affected by host genotype, suggesting differences among the host genotypes in their ability to photo-protect algal symbionts (ANOVA, $F_{1,34} = 4.74$, $P < 0.05$). Meanwhile, both symbiont genotype and growth irradiance affected the first coefficient (ANOVA, $F_{3,32} = 5.56$, $P < 0.01$); and symbiont genotype affected the second coefficient (ANOVA, $F_{1,34} = 8.932$, $P < 0.01$) (see Data S1 for full statistical output). Higher levels of NSV and steeper NSV reaction norms for the 186b *Chlorella*, particularly in its native host background, are consistent with the greater investment in photosynthetic machinery observed in the metabolome, allowing this genotype to better dissipate excess light energy as heat whilst not compromising photosynthetic efficiency.

Mixotrophic photosymbioses are common and play a vital role in biogeochemical cycling in terrestrial and aquatic ecosystems [30–32]. Their breakdown, often driven by environmental change, can be rescued by partner-switching to restore symbiotic function [33,34]. Our findings suggest that convergence among independent symbiotic origins upon a shared primary symbiotic nutrient exchange enables partner-switching between genetically divergent clades. This stands in contrast to the diversity of exchange metabolites used in photosymbioses more broadly. For example, just amongst photosymbiotic cnidaria (i.e. corals, anemones, jellyfish) organic carbon transfer from symbiont to host occurs in the form of glycerol, glucose, maltose, and a variety of lipids and amino acids [35]. Thus, while a variety of potential metabolic solutions to the photosymbiotic nutrient exchange exist, perhaps explaining the abundance and diversity of photosymbioses, within specific symbiotic interactions the optimal solution may be more constrained, resulting in evolutionary convergence among independent originations. The concurrent divergence in algal

photophysiology allowed hosts, through partner-switching, to acquire symbionts with different properties, potentially enabling adaptation to new environments. Crucially, symbiont replacement providing hosts with new adaptive traits is critical in natural populations responding to environmental change; for example, reinfection of corals by thermally tolerant symbionts enables recovery following thermal bleaching events [36–38]. Finally, we observed differences among the *P. bursaria*-*Chlorella* clades in their division of labour between host and symbiont contributions to photoprotection. This may be a common feature of photosymbioses [39,40], for example some pelagic zooplankton and jellyfish hosts adopt behavioural strategies to photoprotect algal symbionts [41], and could be a key mechanism of host-symbiont specificity by mediating genotype by genotype by environment interactions. Host-symbiont specificity and partner-switching are common features of many symbioses [42–46] suggesting that our findings are likely to be of wider relevance beyond photosymbioses. Multiple independent evolutionary origins have occurred in diverse symbiotic relationships [18–21]. While this suggests a strong selective imperative for these symbioses, it may also provide important adaptive potential through functional divergence among originations enabling their resilience to environmental change.

Acknowledgements

This work was funded by grant NE/K011774/2 from the Natural Environment Research Council, UK to MAB, CDL, DDC, and AJW, and a White Rose DTP studentship from the Biotechnology and Biological Sciences Research Council, UK to MESS (BB/M011151/1). The funders had no role in the design of the study, the

223 collection, analysis and interpretation of data, or the writing of the manuscript. We
224 are grateful to Heather Walker for assistance.

Author contributions

225 MB, DC, MS, EM, CL conceived and designed the study. MS and EM conducted
226 experimental work. MS, CL and DC analysed the data. MS and MB drafted the
227 manuscript. All authors commented on the manuscript.

Conflict of interest

228 The authors declare that they have no conflicting interests.

229

230

231

232

233

234

235

236

237

238

Figure Legends

Figure 1: Correlated metabolite enrichment for the 186b and HA1 *Paramecium bursaria* and *Chlorella* strains over time.

Each data point represents a metabolite. In each scatterplot the mean Random Forest rank order of each metabolite in the HA1 strain is plotted against the mean rank order of each metabolite in the 186b strain. The rank order value is positively correlated with magnitude of the enrichment signal. For all panels, the mean rank order is derived from multiple Random Forest analyses (n=500), for further details regarding the Random Forest models see the methods section. A,C,E,G.) N¹⁵ enrichment in the *Chlorella* fraction at 15, 120, 240 and 360 minutes. B,D,F,H.) C¹³ enrichment in the *P. bursaria* fraction at 15, 120, 240 and 360 minutes.

Figure 2: Fitness of the native and non-native host-symbiont pairings relative to isogenic symbiont-free hosts.

Lines show mean (n=3) competitive fitness of symbiont-containing hosts relative to their isogenic symbiont-free host genotype calculated as selection rate, the shaded area denotes \pm SE. The left-hand panel shows data for the HA1 *Paramecium* host genotype, the right-hand panel shows data for the 186b *Paramecium* host genotype containing either native (solid line) or non-native (dashed line) *Chlorella* symbiont genotypes, which are distinguished by colour (186b *Chlorella* in blue; HA1 *Chlorella* in green). Selection rate = 0 represents equal fitness.

Figure 3: Differences in *Chlorella* global metabolism between strains across light conditions.

Comparisons of unlabelled *Chlorella* metabolites between strains and light conditions are represented as volcano plots (A-D) plotting the fold change of each metabolite against its statistical significance. The data points are highlighted at two false discovery rate (FDR) values, and if the $\text{Log}_2(\text{fold change})$ is greater than 1 or less than -1 as indicated in the graphical key. A.) Comparing metabolites between the two strains within the high light condition. B.) Comparing metabolites between the two strains within the low light condition. C.) Comparing metabolites between the two light levels within the HA1 strain. D.) Comparing metabolites between the two light levels within the 186b strain. See Figure S2 for the equivalent plot for the *P. bursaria* metabolite comparisons. Differential metabolites distinguishing the divergent strategies of light management between the two host-symbiont strains were then plotted separately: The relative abundance of the metabolites is plotted within the two strains at the two light conditions. The top three panels (E-G) show metabolites that have been identified as carotenoids and the lower three panels (H-J) show metabolites that have been identified as either chlorophyll or ubiquinone compounds. For panels E-J, responses are presented as the mean ($n=12$) \pm SE and host-symbiont strain is denoted by colour (186b in blue; HA1 in green).

Figure 4: Photophysiology measurements for the native and non-native host-symbiont pairings.

For all subplots, lines represent the mean ($n=3$), the shaded area denotes \pm SE. In each subplot the left-hand panel shows data for the HA1 *Paramecium* host genotype, the right-hand panel shows data for the 186b *Paramecium* host genotype containing either native (solid line) or non-native (dashed line) *Chlorella* symbiont genotypes, which are distinguished by colour (186b *Chlorella* in blue; HA1 *Chlorella*

289 in green). A) Estimates of the maximum quantum yield of photosystem II (F_v/F_m)
290 across growth irradiances. B) Light-adapted quantum yield of photosystem II (Φ_{PSII})
291 across growth irradiances, lines represent exponential decay models using nlme
292 package in R. C.) The normalised Stern-Volmer quenching coefficient ($NSV = F_o'/F_v'$)
293 across growth irradiances, presented at polynomial model fits. See Data S1 for
294 model details.

295

296

297 **STAR Methods**

298 LEAD CONTACT AND MATERIALS AVAILABILITY

299 Further information and requests for resources and reagents should be directed to
300 and will be fulfilled by the Lead Contact, Michael Brockhurst
301 (m.brockhurst@sheffield.ac.uk). These resources and reagents will be made
302 available upon request.

303

304 EXPERIMENTAL MODEL AND SUBJECT DETAILS

305

306 Symbiotic *Paramecium bursaria* stock cultures were maintained at 25°C under a
307 14:10 L:D cycle with 50 $\mu\text{E m}^{-2} \text{s}^{-1}$ of light. Grown in bacterized Protozoan Pellet
308 Media (PPM, Carolina Biological Supply), made to a concentration of 0.66 g L⁻¹ with
309 Volvic natural mineral water, and inoculated approximately 20 hours prior to use with
310 *Serratia marcescens* from frozen glycerol stocks. The two natural strains used were:
311 186b (CCAP 1660/18) obtained from the Culture Collection for Algae and Protozoa
312 (Oban, Scotland), and HA1 isolated in Japan and obtained from the Paramecium
313 National Bio-Resource Project (Yamaguchi, Japan).

314

315 To isolate *Chlorella* from the symbiosis, symbiotic cultures were first washed and
316 concentrated with a 11 μm nylon mesh using sterile Volvic. The suspension was then
317 ultra-sonicated using a Fisherbrand™ Q500 Sonicator (Fisher Scientific, NH, USA),
318 at a power setting of 20% for 10 seconds sonification to disrupt the host cells. The
319 liquid was then spotted onto Bold Basal Media plates (BBM) [47], from which green
320 colonies were streaked out and isolated over several weeks. Plate stocks were
321 maintained by streaking out one colony to a fresh plate every 3/4 weeks.

322

Symbiont-free *P. bursaria* were made by treating symbiotic cultures with paraquat (10 $\mu\text{g mL}^{-1}$) for 3 to 7 days in high light conditions ($>50 \mu\text{E m}^{-2} \text{s}^{-1}$), until the host cells were visibly symbiont free. The cultures were then extensively washing with Volvic and closely monitored with microscopy to check that re-greening by *Chlorella* did not occur. Stock cultures of the symbiont-free cells were maintained by batch culture at 25°C under a 14:10 L:D cycle with $3 \mu\text{E m}^{-2} \text{s}^{-1}$ of light and were given fresh PPM weekly.

METHOD DETAILS

Cross Infections

Symbiont-free populations of the two *P. bursaria* strains were re-infected by adding a colony of *Chlorella* from the plate stocks derived from the appropriate strain. The re-greening process was followed by microscopy and took between 2-6 weeks. Over the process, cells were grown at the intermediate light level of $12 \mu\text{E m}^{-2} \text{s}^{-1}$ and were given bacterized PPM weekly.

Diagnostic PCR

The correct algae genotype was confirmed using diagnostic PCR. The *Chlorella* DNA was extracted by isolating the *Chlorella* and then using a standard 6% Chelex100 resin (Bio-Rad) extraction method. ISSR primer '65' were established for *Chlorella vulgaris* by Shen (2008), and was used as described therein. Standard PCR reactions were performed using Go Taq Green Master Mix (Promega) and $0.5 \mu\text{mol L}^{-1}$ of primer. The thermocycler programme was set to: 94°C for 5min, 40 cycles of (94°C for 20sec, 55°C for 1 min, 72°C for 20sec), and 6 min at 72°C.

349 *Fitness assay*

350 *P. bursaria* cultures, both the symbiotic cross-infections and symbiont-free cells,
351 were washed with Volvic and resuspended in bacterized PPM. The cultures were
352 then split and acclimated at their treatment light level (0,12,50 $\mu\text{E m}^{-2} \text{s}^{-1}$) for five
353 days. Cell densities were counted by fixing 360 μL of each cell culture, in triplicate, in
354 1% v/v glutaraldehyde in 96-well flat bottomed micro-well plates. Images were taken
355 with a plate reader (Tecan Spark 10M) and cell counts were made using an
356 automated image analysis macro in ImageJ v1.50i [49]. The competitions were
357 started with the target values of 20 green cells and 20 white cells per ml. Cells were
358 sampled on day 0 and day 7 and the proportion of green to white cells was
359 measured using flow cytometry analysis. Green versus white cells were
360 distinguished using single cell fluorescence estimated using a CytoFLEX S flow
361 cytometer (Beckman Coulter Inc., CA, USA) by measuring the intensity of chlorophyll
362 fluorescence (excitation 488nm, emission 690/50nm) and gating cell size using
363 forward side scatter [23]. The measurements were calibrated against 8-peak rainbow
364 calibration particles (BioLegend), and then presented as relative fluorescence to
365 reduce variation across sampling sessions.

366

367 *Fluorimetry*

368 The cells were washed and concentrated with a 11 μm nylon mesh using sterile
369 Volvic and re-suspended in bacterized PPM. The cultures were then split and
370 acclimated to their treatment light condition (12, 24 & 50 $\mu\text{E m}^{-2} \text{s}^{-1}$) for five days.
371 F_v/F_m , Φ_{PSII} , and NSV values were measured by fast repetition rate fluorimetry
372 (FastPro8, Chelsea instruments fluorometer [50] following the manufacturer's
373 procedure). Cultures were dark acclimated for 15 minutes prior to measurements.

For maximum quantum yield, measurements were repeated until F_v/F_m stabilized (typically 3-5 minutes) and F_v/F_m then estimated as an average of 10 measurements. Φ_{PSII} was measured in response to an actinic light source at sequentially increasing irradiances between 0 – 2908 PFD following standard green algae protocol. Peak emission wavelengths of the LED used for excitations was 450nm. Non-photochemical quenching was estimated by the normalised Stern-Volmer coefficient, defined as $NSV = F_o'/F_v'$ [51] and corrects for differences in F_v/F_m between samples.

Metabolomics

Cultures were washed and concentrated with a 11 μ m nylon mesh using Volvic and re-suspended in bacterized PPM. The cultures were first grown for three days at 50 μ E m⁻² s⁻¹ to increase cell densities, and then split and acclimated at their treatment light condition (6 & 50 μ E m⁻² s⁻¹) for three days. For the sampling, the cultures were split into 3 treatment: the control, N¹⁵ enrichment by the addition of labelled *Serratia marcescens* (100 μ l per microcosm), or C¹³ enrichment by the addition of HC¹³O₃ (100 mg L⁻¹). The cultures were sampled at four time points (15, 120, 360, 480 minutes after the enrichment event). There were three biological replicates for each sampling event.

At each sampling event, the symbiotic partners were separated in order to get *P. bursaria* and *Chlorella* metabolic fraction. The *P. bursaria* cells were concentrated with a 11 μ m nylon mesh using Volvic and then the *P. bursaria* cells were disrupted by sonication (20% power for 10 secs). 1ml of the lysate was pushed through a 1.6 μ m filter, which caught the intact *Chlorella* cells, and the run-through was collected and stored as the *P. bursaria* fraction. The 1.6 μ m filter was washed with

5ml cold deionized water, and then reversed so that the *Chlorella* cells were resuspended in 1ml of cold methanol, which was stored as the *Chlorella* fraction.

The samples were analysed with a Synapt G2-Si with Acquity UPLC, recording in positive mode over a large untargeted mass range (50 – 1000 Da). A 2.1x50mm Acquity UPLC BEH C18 column was used with acetonitrile as the solvent. The machine settings are listed in detail below:

Mass spectrometry settings:

Polarity:	positive
Capillary voltage:	2.3 kV
Sample Cone voltage:	20 V
Source Temperature:	100°C
Desolvation temperature:	280°C
Gas Flow:	600 L hr ⁻¹
Injected volume:	5µl

Gradient information:

Time (mins)	Water (%)	Acetonitrile (%)
0	95	5
3	65	35
6	0	100
7.5	0	100
7.6	95	5

The *P. bursaria* and *Chlorella* fraction were analysed separately. The xcms R package [52–54] was used for automatic peak detection by extracting the spectra

from the CDF data files, using a step argument of 0.01 m/z. The automatically identified peaks were grouped across samples and were used to identify and correct correlated drifts in retention time from run to run. Pareto scaling was applied to the resulting intensity matrix.

Isotope analysis

For the *P. bursaria* isotope analysis the C¹³ labelled samples were compared with the control, while for the *Chlorella* analysis the N¹⁵ labelled samples were compared to the control. In order to identify isotopic enrichment without user bias, we used Random Forest (RF) models to identify metabolites that associated with the isotope labelling. This is a machine-learning decision-tree based approach that produces powerful multivariate regression and is an established method for high-throughput biological data [55], including metabolomics [56]. The isotope label was used as the response variable to regress against the metabolic profile of each sample. Each random forest model was run with 1000 iterations, and each RF analysis was run 500 times to account for uncertainty in the rank score. For each run, the rank score of the RF importance (measured as the mean decrease in Gini) was recorded for each m/z bin. The mean and standard error of the rank score was then calculated to assess the consistency of the variable importance. In total 4 RF models were analysed within each fraction, 1 per timepoint.

The rank score values were then compared between the strains. The co-enriched metabolites were filtered to select those that had a higher relative abundance in the labelled fraction than in the control. From these, the profile of each candidate metabolite was manually checked for isotopic enrichment, and when a clear

enrichment profile was present the monoisotopic mass was identified. The enrichment proportion of the isotopic masses to the monoisotopic mass was calculated, and the natural enrichment value within the control fraction was subtracted from the enrichment in the labelled fraction. Following this calculation, it was possible to determine if enrichment had occurred, and if so, the monoisotopic mass was considered a 'mass of interest'.

Target Pathway analysis

Given that the low molecular weight compounds in the results of the ^{15}N co-enrichment in *Chlorella* (Table S2) were almost exclusively amino acid or purine related, we focused on these pathways for a further targeted approach. Key compounds of these pathways were selected and searched for in the metabolite dataset. To follow the flow of enriched nitrogen in these pathways, the relative enrichment profile of these compounds compared to the control fraction was calculated. The results were visualised as heatmaps, with the heatmap.2() function from the gplot package [57], based on the method used by Austen et al. (In Press).

Some of the amino acid metabolism results are plotted in Figure S4 and show that the nitrogen enrichment is focused downstream from arginine. Other aspects of amino acid metabolism, such as that centred around aspartate, serine or lysine, showed little and inconsistent enrichment. Within purine metabolism, the nitrogen enrichment occurred both up and downstream of the purine bases. The enrichment upstream of the purine bases indicates that enriched nitrogen is entering this pathway from the amino acid of central metabolism. Based on this pattern, we

believe that the purine pathway is a site of secondary enrichment and it reveals that purine-derivatives present a substantial nitrogen demand.

Unfortunately, we could not identify a candidate compound for arginine to test if it had the enrichment profile of a transfer molecule (predicted to be a very high initial enrichment that then substantially decreased over time). Such a pattern was not seen for any compound, we suggest, therefore, that our first timepoint was not early enough to capture the initial enrichment events involving the transfer compound itself.

Unlabelled analysis

For the unlabelled, control fraction, metabolite relative abundance was compared between the strains by calculating the log₂(Fold Change) between the conditions (either between the strains within each light level, or between the light levels within each strain) in a series of pair-wise contrasts for each metabolite. Student T-tests were performed between the relative abundances of the paired comparisons. The *Benjamini–Hochberg* procedure was used to account for the high number of multiple P-value comparisons, with the false discovery rate set to 0.1 and 0.05 [58] as highlighted in the volcano plots.

Identification of significant masses

Masses of interest were investigated using the MarVis-Suite 2.0 software (<http://marvis.gobics.de/>) [59], using retention time and mass to compare against KEGG (<https://www.genome.jp/kegg/>) [60,61] and MetaCyc (<https://biocyc.org/>) [62] databases. The Metabolomics Standards Initiative requires two independent

measures to confirm identity, which the combination of retention time and accurate mass achieves. This analysis therefore confirms level 1 identification.

QUANTIFICATION AND STATISTICAL ANALYSIS

Statistical analyses were performed in R v.3.5.0 [63] and all plots were produced using package ggplot2 [64]. Physiology tests were analysed by both ANOVA and ANCOVA, with light, host and symbiont identity as factors. Φ_{PSII} results were analysed with non-linear mixed effects models (nlme) with the nlme R package [65]. The Φ_{PSII} data was fitted to an exponential decay function:

$$\Phi_{PSII} = ae^{(bt)}$$

Where a is a normalisation constant and b is the rate constant. The nlme model included random effects for replicate on each parameter and fixed factors of host, symbiont and light factors and their interactions with a following model reduction. See the full statistics table (Data S1) for further details on the statistics used.

DATA AND CODE AVAILABILITY

The data has been deposited within Mendeley Data (DOI: 10.17632/6zspctmwpj.1).

520 **Legends for supplementary datasets**

521

522 **Data S1. Statistical outputs for analyses associated with the figures of the**
523 **main manuscript. Related to Figure 2 and 5**

524

525 **References:**

- 526 1. Wernegreen, J.J. (2012). Endosymbiosis. *Current Biology* 22, R555–R561.
- 527 2. Sudakaran, S., Kost, C., and Kaltenpoth, M. (2017). Symbiont Acquisition and
528 Replacement as a Source of Ecological Innovation. *Trends in Microbiology* 25, 375–390.
- 529 3. Kiers, E.T., and West, S.A. (2015). Evolving new organisms via symbiosis. *Science* 348,
530 392–394.
- 531 4. Powell, J.R., and Rillig, M.C. (2018). Biodiversity of arbuscular mycorrhizal fungi and
532 ecosystem function. *New Phytol.*
- 533 5. Baker, A.C. (2003). Flexibility and Specificity in Coral-Algal Symbiosis: Diversity,
534 Ecology, and Biogeography of Symbiodinium. *Annual Review of Ecology, Evolution,*
535 *and Systematics* 34, 661–689.
- 536 6. Zook, D.P. (2002). Prioritizing Symbiosis to Sustain Biodiversity: Are Symbionts
537 Keystone Species? In *Symbiosis: Mechanisms and Model Systems Cellular Origin, Life*
538 *in Extreme Habitats and Astrobiology.*, J. Seckbach, ed. (Dordrecht: Springer
539 Netherlands), pp. 3–12.
- 540 7. Sachs, J.L., Skophammer, R.G., and Regus, J.U. (2011). Evolutionary transitions in
541 bacterial symbiosis. *PNAS* 108, 10800–10807.
- 542 8. Moran, N.A., and Wernegreen, J.J. (2000). Lifestyle evolution in symbiotic bacteria:
543 insights from genomics. *Trends in Ecology & Evolution* 15, 321–326.
- 544 9. Fujishima, M., and Kodama, Y. (2012). Endosymbionts in Paramecium. *European*
545 *Journal of Protistology* 48, 124–137.
- 546 10. Hoshina, R., and Imamura, N. (2008). Multiple Origins of the Symbioses in Paramecium
547 bursaria. *Protist* 159, 53–63.
- 548 11. Summerer, M., Sonntag, B., and Sommaruga, R. (2008). Ciliate-Symbiont Specificity of
549 Freshwater Endosymbiotic Chlorella (trebouxiophyceae, Chlorophyta)1. *Journal of*
550 *Phycology* 44, 77–84.
- 551 12. Kato, Y., Ueno, S., and Imamura, N. (2006). Studies on the nitrogen utilization of
552 endosymbiotic algae isolated from Japanese Paramecium bursaria. *Plant Science* 170,
553 481–486.
- 554 13. Kessler, E., and Huss, V. a. R. (1990). Biochemical Taxonomy of Symbiotic Chlorella
555 Strains from Paramecium and Acanthocystis*. *Botanica Acta* 103, 140–142.
- 556 14. Johnson, M.D. (2011). The acquisition of phototrophy: adaptive strategies of hosting
557 endosymbionts and organelles. *Photosynth Res* 107, 117–132.
- 558 15. Ziesenisz, E., Reisser, W., and Wiessner, W. (1981). Evidence of de novo synthesis of
559 maltose excreted by the endosymbiotic Chlorella from Paramecium bursaria. *Planta* 153,
560 481–485.

- 561 16. Sachs, J.L., and Simms, E.L. (2006). Pathways to mutualism breakdown. Trends in
562 Ecology & Evolution 21, 585–592.
- 563 17. Herre, E.A., Knowlton, N., Mueller, U.G., and Rehner, S.A. (1999). The evolution of
564 mutualisms: exploring the paths between conflict and cooperation. Trends in Ecology &
565 Evolution 14, 49–53.
- 566 18. Muggia, L., Nelson, P., Wheeler, T., Yakovchenko, L.S., Tønsberg, T., and Spribille, T.
567 (2011). Convergent evolution of a symbiotic duet: The case of the lichen genus
568 Polychidium (Peltigerales, Ascomycota). American Journal of Botany 98, 1647–1656.
- 569 19. Masson-Boivin, C., Giraud, E., Perret, X., and Batut, J. (2009). Establishing nitrogen-
570 fixing symbiosis with legumes: how many rhizobium recipes? Trends in Microbiology
571 17, 458–466.
- 572 20. Boscaro, V., Husnik, F., Vannini, C., and Keeling, P.J. (2019). Symbionts of the ciliate
573 Euplotes: diversity, patterns and potential as models for bacteria–eukaryote
574 endosymbioses. Proceedings of the Royal Society B: Biological Sciences 286, 20190693.
- 575 21. Hulcr, J., and Stelinski, L.L. (2017). The Ambrosia Symbiosis: From Evolutionary
576 Ecology to Practical Management. Annual Review of Entomology 62, 285–303.
- 577 22. Zagata, P., Greczek-Stachura, M., Tarcz, S., and Rautian, M. (2016). The Evolutionary
578 Relationships between Endosymbiotic Green Algae of Paramecium bursaria Syngens
579 Originating from Different Geographical Locations. Folia Biologica 64, 47–54.
- 580 23. Kadono, T., Kawano, T., Hosoya, H., and Kosaka, T. (2004). Flow cytometric studies of
581 the host-regulated cell cycle in algae symbiotic with green paramecium. Protoplasma
582 223, 133–141.
- 583 24. Soldo, A.T., Godoy, G.A., and Larin, F. (1978). Purine-Excretory Nature of Refractile
584 Bodies in the Marine Ciliate Parauronema acutum*. The Journal of Protozoology 25,
585 416–418.
- 586 25. Shah, N., and Syrett, P.J. (1984). The uptake of guanine and hypoxanthine by marine
587 microalgae. Journal of the Marine Biological Association of the United Kingdom 64,
588 545–556.
- 589 26. Quispe, C.F., Sonderman, O., Khasin, M., Riekhof, W.R., Van Etten, J.L., and Nickerson,
590 K.W. (2016). Comparative genomics, transcriptomics, and physiology distinguish
591 symbiotic from free-living Chlorella strains. Algal Research 18, 332–340.
- 592 27. Minaeva, E., and Ermilova, E. (2017). Responses triggered in chloroplast of Chlorella
593 variabilis NC64A by long-term association with Paramecium bursaria. Protoplasma, 1–8.
- 594 28. Arnou, P., Oleson, J.J., and Williams, J.H. (1953). The Effect of Arginine on the
595 Nutrition of Chlorella vulgaris. American Journal of Botany 40, 100–104.
- 596 29. Maxwell, K., and Johnson, G.N. (2000). Chlorophyll fluorescence—a practical guide. J
597 Exp Bot 51, 659–668.

- 598 30. Esteban, G.F., Fenchel, T., and Finlay, B.J. (2010). Mixotrophy in Ciliates. *Protist* 161,
599 621–641.
- 600 31. Stanley, G.D., and Lipps, J.H. (2011). Photosymbiosis: The Driving Force for Reef
601 Success and Failure. *The Paleontological Society Papers* 17, 33–59.
- 602 32. Caron, D.A. (2016). Mixotrophy stirs up our understanding of marine food webs. *PNAS*
603 113, 2806–2808.
- 604 33. Boulotte, N.M., Dalton, S.J., Carroll, A.G., Harrison, P.L., Putnam, H.M., Peplow, L.M.,
605 and van Oppen, M.J. (2016). Exploring the *Symbiodinium* rare biosphere provides
606 evidence for symbiont switching in reef-building corals. *The ISME Journal* 10, 2693–
607 2701.
- 608 34. Lefèvre, C., Charles, H., Vallier, A., Delobel, B., Farrell, B., and Heddi, A. (2004).
609 Endosymbiont Phylogenesis in the Dryophthoridae Weevils: Evidence for Bacterial
610 Replacement. *Mol Biol Evol* 21, 965–973.
- 611 35. Yellowlees, D., Rees, T.A.V., and Leggat, W. (2008). Metabolic interactions between
612 algal symbionts and invertebrate hosts. *Plant, Cell & Environment* 31, 679–694.
- 613 36. Berkelmans, R., and van Oppen, M.J.H. (2006). The role of zooxanthellae in the thermal
614 tolerance of corals: a ‘nugget of hope’ for coral reefs in an era of climate change.
615 *Proceedings of the Royal Society B: Biological Sciences* 273, 2305–2312.
- 616 37. Rowan, R. (2004). Thermal adaptation in reef coral symbionts. *Nature* 430, 742–742.
- 617 38. Kinzie, R.A., Takayama, M., Santos, S.R., and Coffroth, M.A. (2001). The Adaptive
618 Bleaching Hypothesis: Experimental Tests of Critical Assumptions. *The Biological*
619 *Bulletin* 200, 51–58.
- 620 39. Ye, S., Bhattacharjee, M., and Siemann, E. (2019). Thermal Tolerance in Green Hydra:
621 Identifying the Roles of Algal Endosymbionts and Hosts in a Freshwater Holobiont
622 Under Stress. *Microb Ecol* 77, 537–545.
- 623 40. Venn, A.A., Loram, J.E., and Douglas, A.E. (2008). Photosynthetic symbioses in
624 animals. *J Exp Bot* 59, 1069–1080.
- 625 41. Cimino, M.A., Patris, S., Ucham, G., Bell, L.J., and Terrill, E. (2018). Jellyfish
626 distribution and abundance in relation to the physical habitat of Jellyfish Lake, Palau.
627 *Journal of Tropical Ecology* 34, 17–31.
- 628 42. Husnik, F., and McCutcheon, J.P. (2016). Repeated replacement of an intrabacterial
629 symbiont in the tripartite nested mealybug symbiosis. *PNAS* 113, E5416–E5424.
- 630 43. Koga, R., and Moran, N.A. (2014). Swapping symbionts in spittlebugs: evolutionary
631 replacement of a reduced genome symbiont. *The ISME Journal* 8, 1237–1246.
- 632 44. Matsuura, Y., Moriyama, M., Łukasik, P., Vanderpool, D., Tanahashi, M., Meng, X.-Y.,
633 McCutcheon, J.P., and Fukatsu, T. (2018). Recurrent symbiont recruitment from fungal
634 parasites in cicadas. *PNAS* 115, E5970–E5979.

- 635 45. Sepp, S.-K., Davison, J., Jairus, T., Vasar, M., Moora, M., Zobel, M., and Öpik, M.
636 (2019). Non-random association patterns in a plant–mycorrhizal fungal network reveal
637 host–symbiont specificity. *Molecular Ecology* 28, 365–378.
- 638 46. Parker, B.J., Hřček, J., McLean, A.H.C., and Godfray, H.C.J. (2017). Genotype
639 specificity among hosts, pathogens, and beneficial microbes influences the strength of
640 symbiont-mediated protection. *Evolution* 71, 1222–1231.
- 641 47. Stein, J.R. (1979). (ED.) *Handbook of Phycological Methods: Culture Methods and*
642 *Growth Measurements* (Cambridge University Press).
- 643 48. Shen, S. (2008). Genetic diversity analysis with ISSR PCR on green algae <Emphasis
644 Type="Italic">*Chlorella vulgaris*</Emphasis> and <Emphasis Type="Italic">*Chlorella*
645 *pyrenoidosa*</Emphasis>. *Chin. J. Ocean. Limnol.* 26, 380–384.
- 646 49. Schneider, C.A., Rasband, W.S., and Eliceiri, K.W. (2012). NIH Image to ImageJ: 25
647 years of image analysis. *Nature Methods*.
- 648 50. Oxborough, K., Moore, C.M., Suggett, D.J., Lawson, T., Chan, H.G., and Geider, R.J.
649 (2012). Direct estimation of functional PSII reaction center concentration and PSII
650 electron flux on a volume basis: a new approach to the analysis of Fast Repetition Rate
651 fluorometry (FRRf) data. *Limnology and Oceanography: Methods* 10, 142–154.
- 652 51. McKew, B.A., Davey, P., Finch, S.J., Hopkins, J., Lefebvre, S.C., Metodiev, M.V.,
653 Oxborough, K., Raines, C.A., Lawson, T., and Geider, R.J. (2013). The trade-off between
654 the light-harvesting and photoprotective functions of fucoxanthin-chlorophyll proteins
655 dominates light acclimation in *Emiliania huxleyi* (clone CCMP 1516). *New Phytologist*
656 200, 74–85.
- 657 52. Benton, H.P., Want, E.J., and Ebbels, T.M.D. (2010). Correction of mass calibration gaps
658 in liquid chromatography-mass spectrometry metabolomics data. *Bioinformatics* 26,
659 2488–2489.
- 660 53. Smith, C.A., Want, E.J., O’Maille, G., Abagyan, R., and Siuzdak, G. (2006). XCMS:
661 Processing Mass Spectrometry Data for Metabolite Profiling Using Nonlinear Peak
662 Alignment, Matching, and Identification. *Anal. Chem.* 78, 779–787.
- 663 54. Tautenhahn, R., Böttcher, C., and Neumann, S. (2008). Highly sensitive feature detection
664 for high resolution LC/MS. *BMC Bioinformatics* 9, 504.
- 665 55. Touw, W.G., Bayjanov, J.R., Overmars, L., Backus, L., Boekhorst, J., Wels, M., and van
666 Hijum, S.A.F.T. (2013). Data mining in the Life Sciences with Random Forest: a walk in
667 the park or lost in the jungle? *Brief. Bioinformatics* 14, 315–326.
- 668 56. Hopkins, D.P., Cameron, D.D., and Butlin, R.K. (2017). The chemical signatures
669 underlying host plant discrimination by aphids. *Scientific Reports* 7, 8498.
- 670 57. Warnes, G.R., Bolker, B., Bonebakker, L., Gentleman, R., Huber, W., Liaw, A., Lumley,
671 T., Maechler, M., Magnusson, A., and Moeller, S. (2009). *gplots: Various R*
672 *programming tools for plotting data.* R package version 2, 1.

673 58. Storey, J.D., and Tibshirani, R. (2003). Statistical significance for genomewide studies.
674 PNAS 100, 9440–9445.

675 59. Kaefer, A., Lingner, T., Feussner, K., Göbel, C., Feussner, I., and Meinicke, P. (2009).
676 MarVis: a tool for clustering and visualization of metabolic biomarkers. BMC
677 Bioinformatics 10, 92.

678 60. Kanehisa, M., and Goto, S. (2000). KEGG: kyoto encyclopedia of genes and genomes.
679 Nucleic Acids Res. 28, 27–30.

680 61. Kanehisa, M., Sato, Y., Furumichi, M., Morishima, K., and Tanabe, M. (2019). New
681 approach for understanding genome variations in KEGG. Nucleic Acids Res. 47, D590–
682 D595.

683 62. Caspi, R., Billington, R., Fulcher, C.A., Keseler, I.M., Kothari, A., Krummenacker, M.,
684 Latendresse, M., Midford, P.E., Ong, Q., Ong, W.K., *et al.* (2018). The MetaCyc
685 database of metabolic pathways and enzymes. Nucleic Acids Res 46, D633–D639.

686 63. R Core Team (2018). R: A Language and Environment for Statistical Computing.
687 Available at: <https://www.R-project.org/>.

688 64. Wickham, H. (2016). ggplot2: Elegant Graphics for Data Analysis.

689 65. Pinheiro, J., Bates, D., DebRoy, S., Sarkar, D., and R core Team (2019) (2019). nlme:
690 Linear and Nonlinear Mixed Effects Models. Available at: [https://CRAN.R-](https://CRAN.R-project.org/package=nlme)
691 [project.org/package=nlme](https://CRAN.R-project.org/package=nlme).

692

693

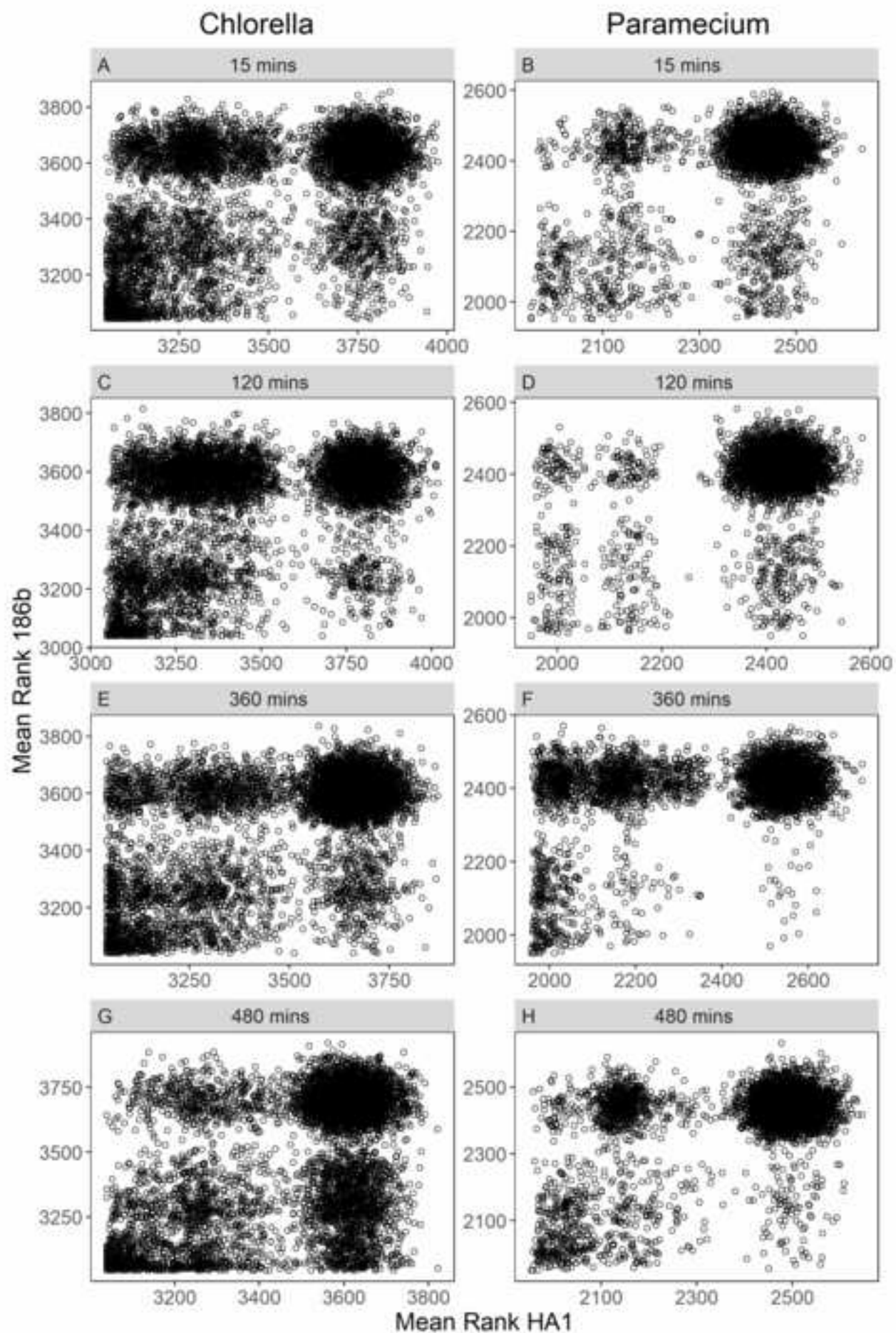
694

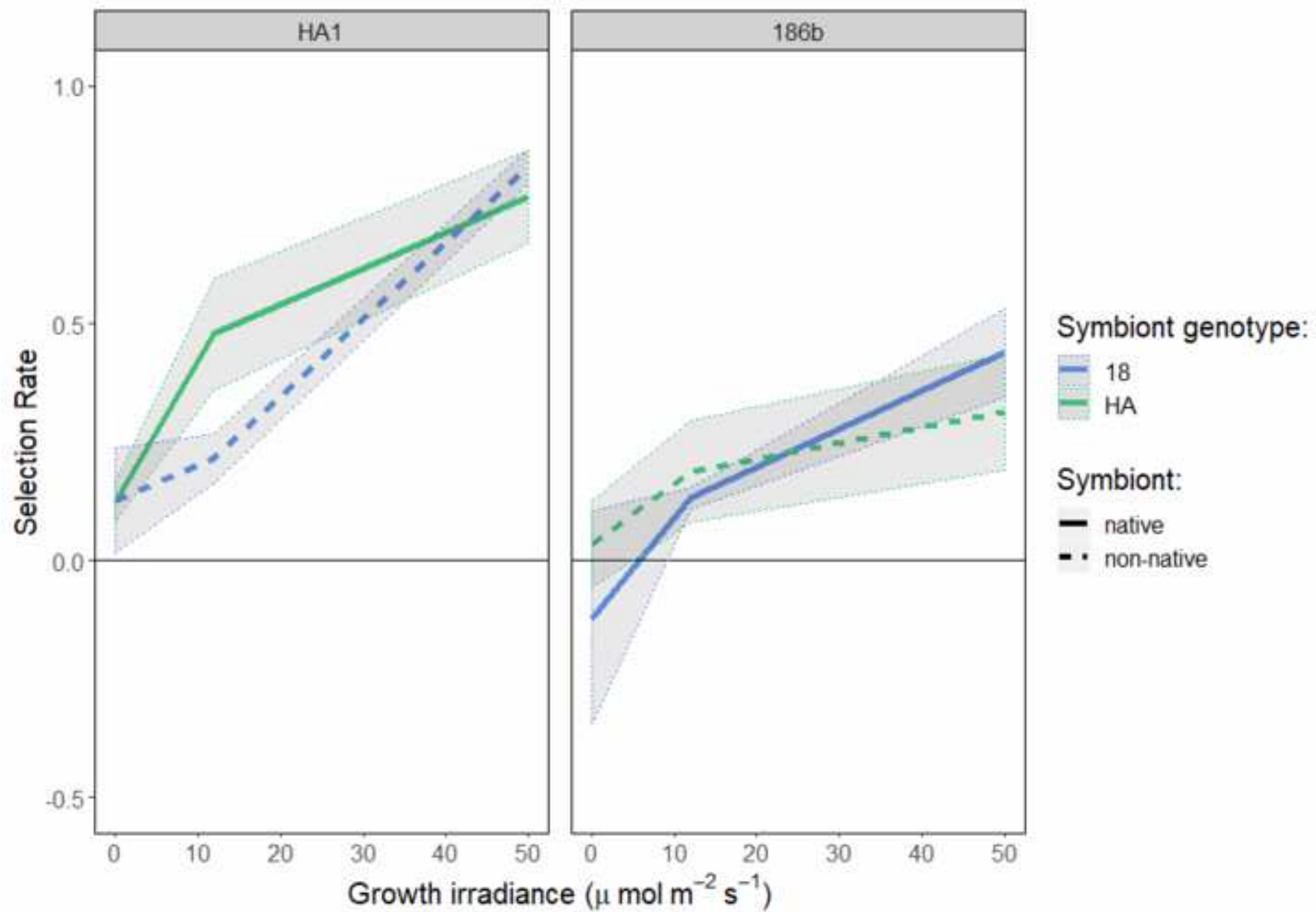
695

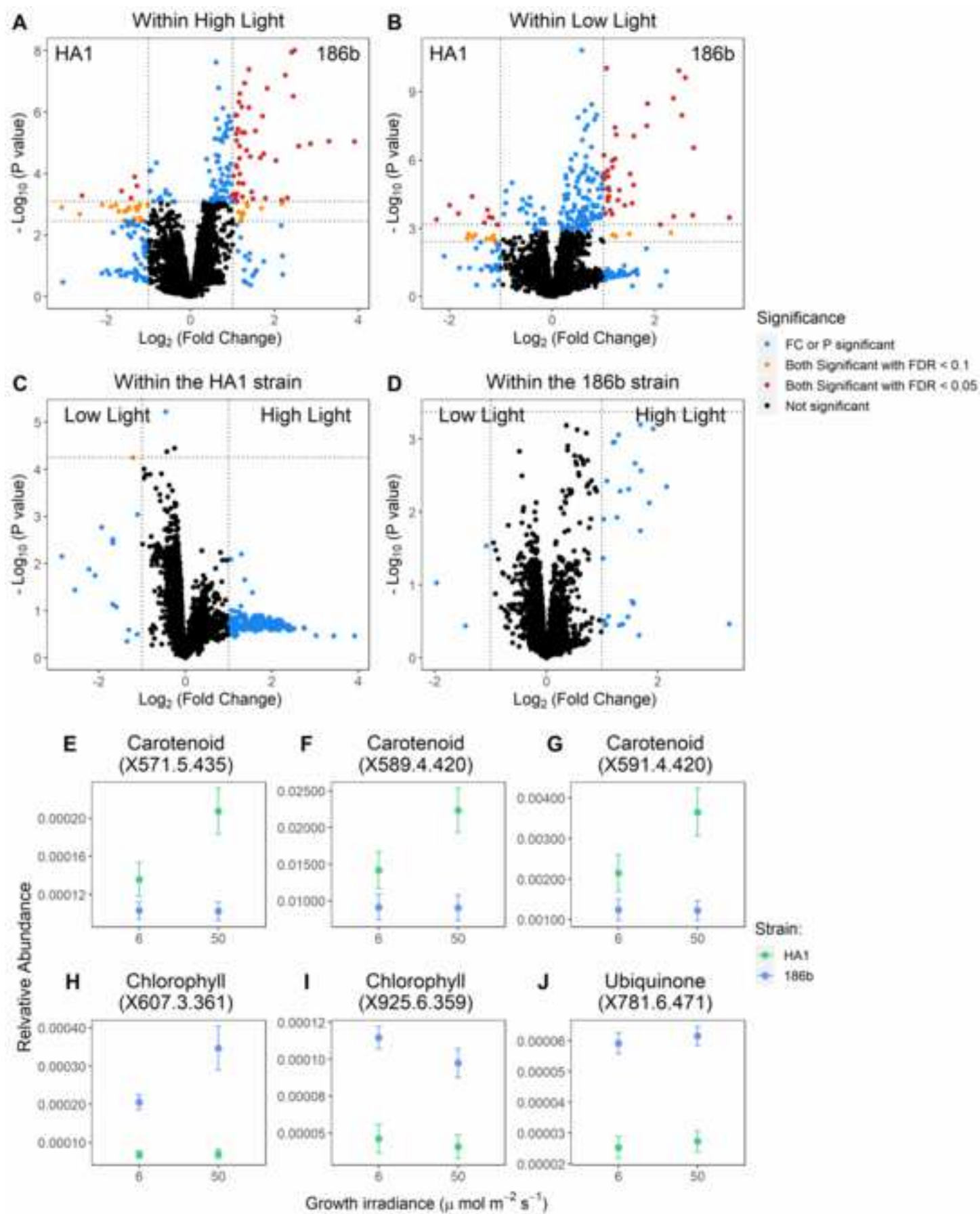
696

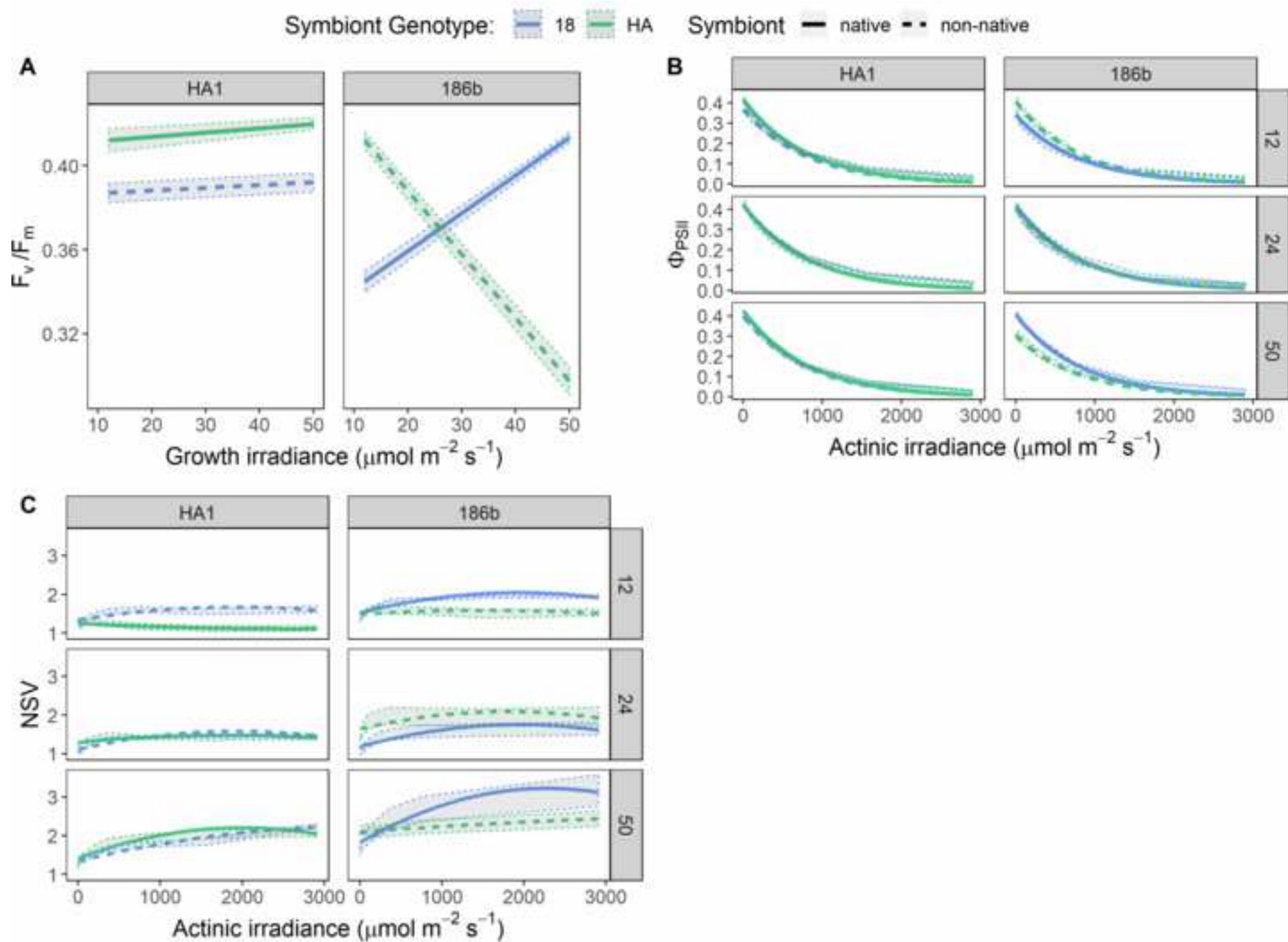
KEY RESOURCES TABLE

REAGENT or RESOURCE	SOURCE	IDENTIFIER
Bacterial and Virus Strains		
<i>Serratia marcescens</i>	Collection of Institut Pasteur	CIP 103235T
Chemicals, Peptides, and Recombinant Proteins		
Protozoan Pellet Media	Carolina Biological Supply	132360
Paraquat dichloride	Sigma-Aldrich	36541; CAS: 75365-73-0
8-peak rainbow calibration particles	BioLegend	422903
Chelex100 resin	Bio-Rad Laboratories	1421253
Deposited Data		
Mass spectrometry data, fluorimetry data and flow cytometry data	This paper	DOI: 10.17632/6zspctmwpj.1
Experimental Models: Organisms/Strains		
<i>P. bursaria</i> – <i>Chlorella</i> 186b strain	Culture Collection of Algae and Protozoa	CCAP 1660/18
<i>P. bursaria</i> – <i>Chlorella</i> HA1 strain	National BioResource project	NBRP ID: PB034004A
Oligonucleotides		
ISSR primer '65': AGAGAGAGAGAGAGAGCC	Shen (2008)	N/A
Software and Algorithms		
ImageJ v1.50i	Schneider et al., 2012	https://imagej.nih.gov/ij/
xcms R package	Benton et al., 2010; Smith et al., 2006; Tanutenhahn et al., 2008	https://bioconductor.org/packages/release/bioc/html/xcms.html
MarVis-Suite 2.0 software	Kaever et al., 2009	http://marvis.gobics.de/









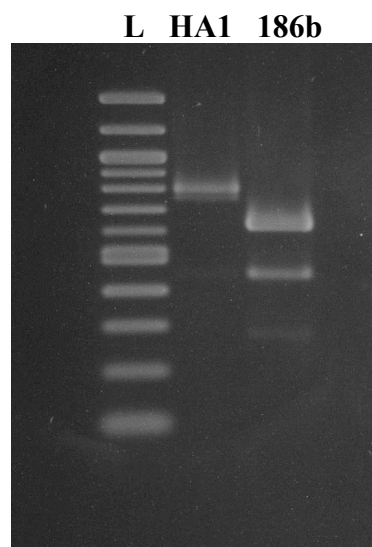


Figure S1: Diagnostic PCR between the HA1 and 186b *Chlorella* strains.

Related to main text.

Showing clear banding pattern differences with the '65 ISSR' primer. Shown with a 100 bp ladder.

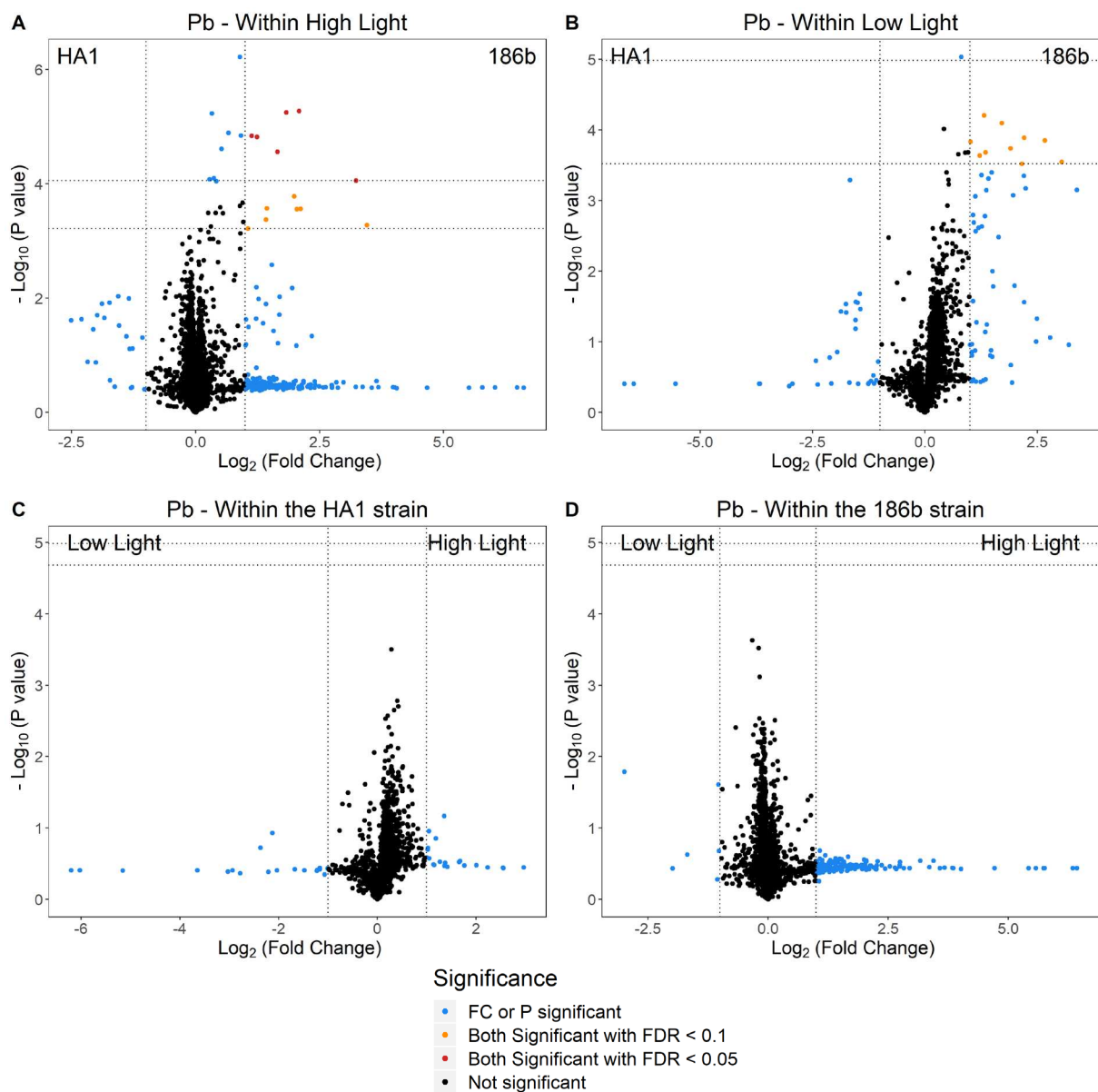


Figure S2: Comparisons of the unlabelled *Parametium* metabolites between the strains and light conditions. Related to Figure 3.

Volcano plots for the unlabelled *Parametium* metabolite comparisons. Plotting the fold change of each metabolite against its statistical significance. The data points are highlighted at two false discovery rate (FDR) values, and if the $\text{Log}_2(\text{fold change})$ is greater than 1 or less than -1. A.) Comparing the expression between the two strains within the high light condition. B.) Comparing the expression between the two strains within the low light condition. C.) Comparing expression between the two light levels within the HA1 strain. D.) Comparing expression between the two light levels within the 186b strain.

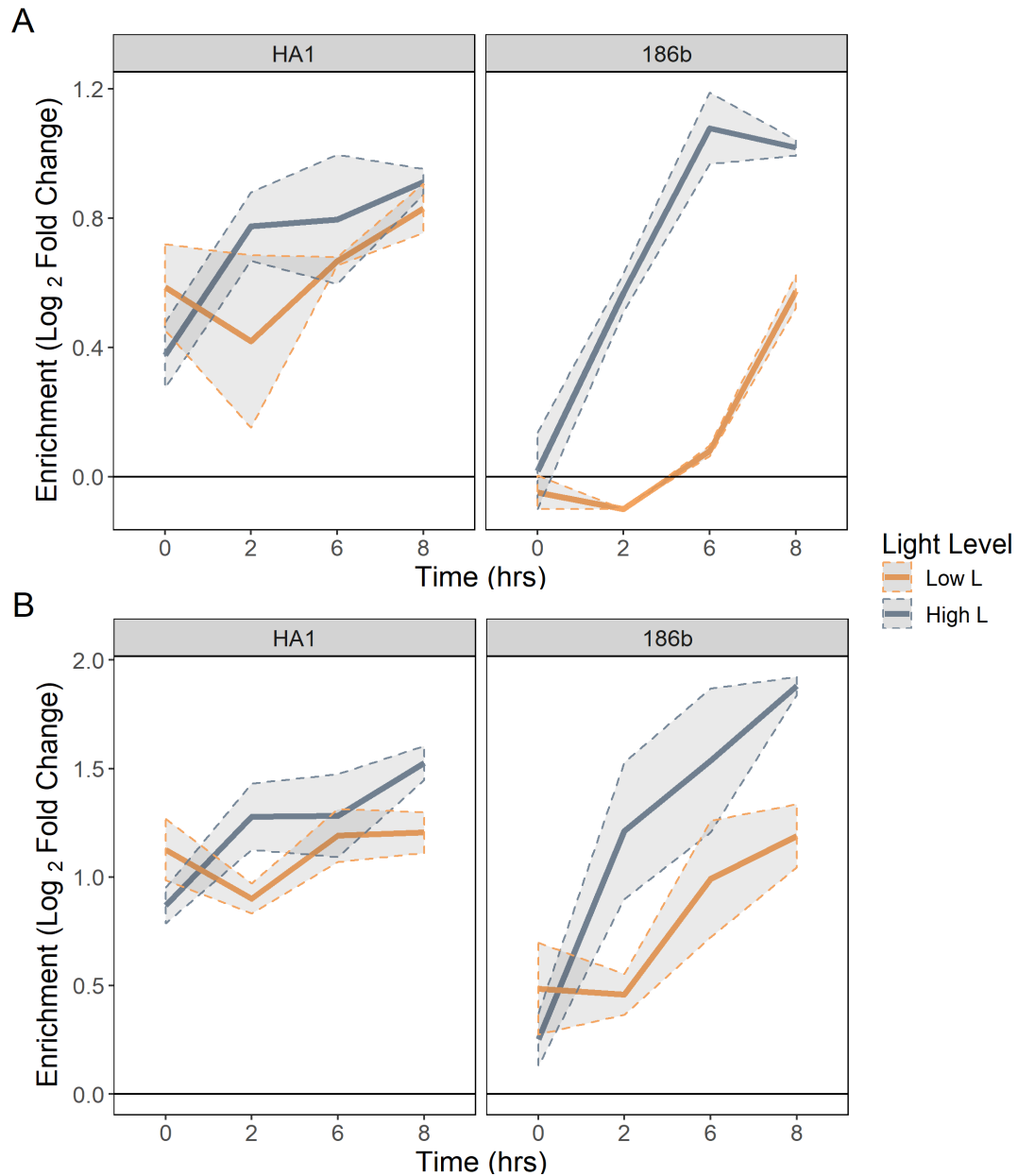


Figure S3: The interaction of light intensity and strain identity on the C¹³ enrichment profile of carbohydrate metabolites in the *Paramecium* fraction. Related to the main text.

For all panels, the enrichment value is the Log₂ of the Fold Change in enrichment of the C¹³ labelled fraction compared to the control. Presented as the mean (n=3) ±SE. The low light level refers to 6 μmol m⁻² s⁻¹ and the high light to 50 μmol m⁻² s⁻¹. A) Profile of 689.2 m/z, 16 rt, Glycogen. B) Profile of 365.1 m/z, 16 rt, a disaccharide, thought to be sucrose.

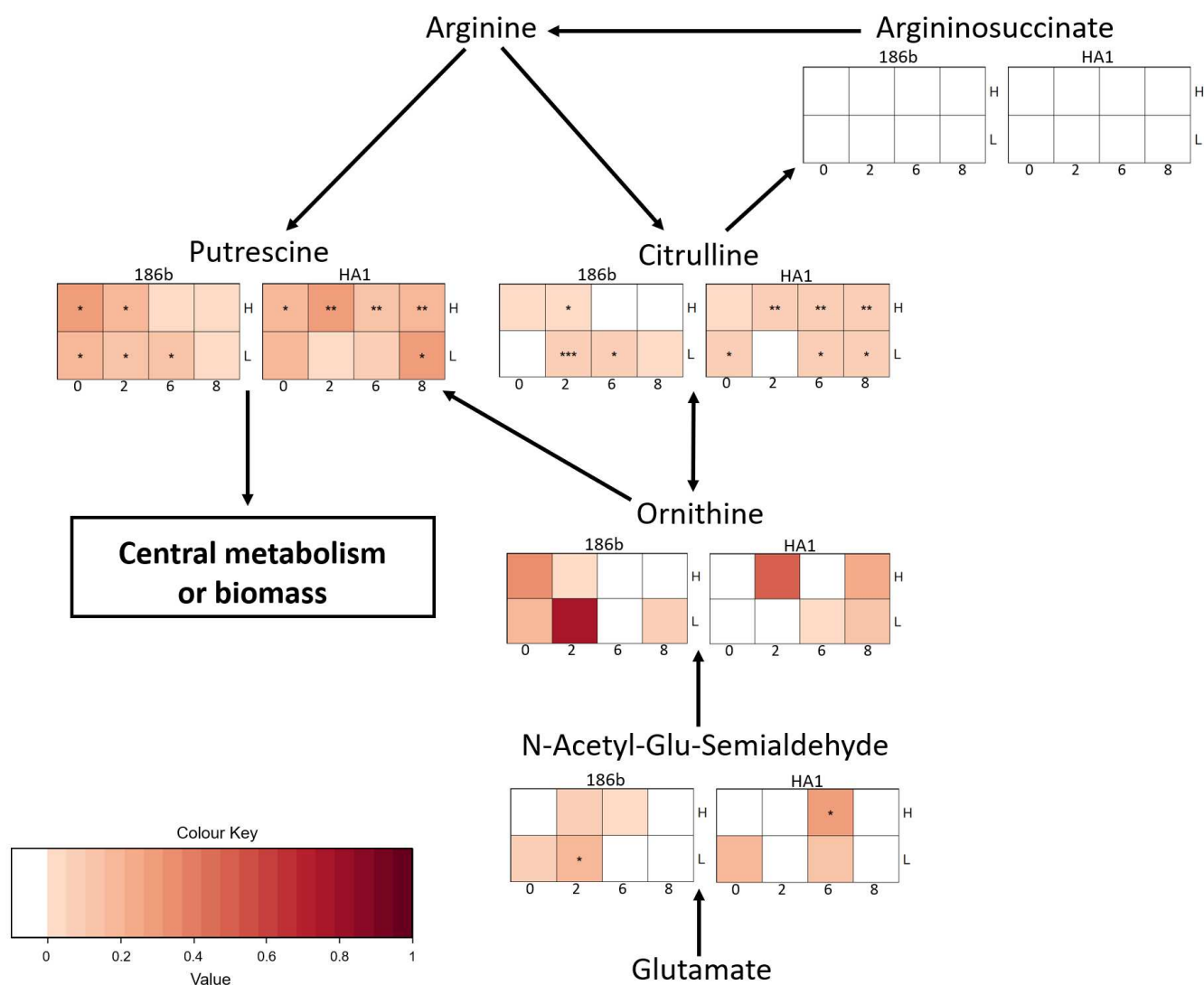


Figure S4: Schematic pathway diagram of nitrogen enrichment in the amino acid metabolism of the *Chlorella* metabolic fraction. Related to the main text and STAR methods.

The tables show relative N¹⁵ enrichment across time (in hrs), in the two light conditions (H = 50 $\mu\text{mol m}^{-2} \text{s}^{-1}$, L = 6 $\mu\text{mol m}^{-2} \text{s}^{-1}$). The colour corresponds to the fold change of the enrichment compared to the control, with significance stars indicating the statistical strength of this change. The nitrogen enrichment is focused downstream from arginine; ornithine, putrescine and citrulline possessed clear enrichment profiles while upstream compounds such as argininosuccinate had no detectable enrichment. This analysis is further explained in the STAR methods section.

Table S1. Details of the *P. bursaria* – *Chlorella* strains. Related to main text.

Strain	Year	Location	Latitude and Longitude	Elevation	Average Temperature Range	Average Total Sunshine hours a year	Culture Collection
186b	2006	Lilly Loch, Inverawe, Scotland, UK	56°26'03.8"N 5°12'22.1"W	20-40m	2.3°C to 17.9°C ¹	1,219.4 hrs ¹	CCAP 1660/18 ²
HA1	2010	Hirosaki-city, Aomori pref, Japan	40°35'35.02"N 140°28'21"E	45m	-5°C to 28°C ³	2013.2 hrs ³	NBRP ID: PB034004A ⁴

¹ Based on the Met Office UK Climate averages data for Dunstaffnage (<https://www.metoffice.gov.uk/research/climate/maps-and-data/uk-climate-averages>)

² https://www.ccap.ac.uk/strain_info.php?Strain_No=1660/18

³ Based on data for Hirosaki city and Aomori airport (<https://www.japanhoppers.com/en/tohoku/hirosaki/weather/>) (<https://www.worldweatheronline.com/hirosaki-weather-averages/aomori/jp.aspx>)

⁴ http://nbrpcms.nig.ac.jp/paramecium/wp-content/themes/paramecium/data/strain_ha1g.pdf

Table S2. List of metabolite IDs found to be co-enriched with N¹⁵ in the *Chlorella* fraction and their candidate identifications. Related to Figure 1.

RF Time	Detected Mass	Retention Time	Pathway	Candidate Compounds	Exact Mass	Adduct	KEGG/ MetaCyc
1	113	482	Pyrimidine/Amino acid	Uracil	112.0273	H+	C00106
				1,3-diaminopropane	74.0844	K+	C00986
1	166	478	Purine	5-Amino-4-imidazole carboxylate	127.0382	K+	C05516
1,2	237.1	286	Biotin	Dethiobiotin	214.1317	Na+	C01909
1,2,3,4	871.6	405	Chlorophyll	Pheophytin A	870.5659	H+	C05797
1,2,4	593.3	405	Chlorophyll	Pheophorbide A	592.2686	H+	C18021
				Urobilinogen	592.3261	H+	C05790
2,3	140	213	Amino acid	L-Aspartate 4-semialdehyde	117.0426	Na+	C00441
				Indole	117.0578	Na+	C00463
				1-Aminocyclopropane-carboxylate	101.0477	K+	C01234
				5-Aminopentanal	101.0841	K+	C12455
3	482.4	324	Folate biosynthesis	Dihydrofolate	443.1553	K+	C00415
3	848.6	294	Ubiquinone	Rhodoquinone-10	847.6842	H+	CPD-9613
4	227.1	460	Amino acid/Chlorophyll	Tryptophan	204.0899	Na+	C00078
				Porphobilinogen	226.0954	H+	C00931

Table S3. List of metabolite IDs found to be co-enriched with C¹³ in the *P. bursaria* fraction and their candidate identifications. Related to Figure 1.

RF Time	Detected Mass	Retention Time	Pathway	Candidate Compounds	Exact Mass	Adduct	KEGG
1	100	16	Glycerophospholipid	Ethanolamine	61.0528	K+	C00189
1	689.2	16	Carbohydrate	Glycogen	666.2219	Na+	C00182
1,2	124	15	Vitamins and Cofactors	Niacin	123.032	H+	C00253
1,2	261	14	Carbohydrate	Monosaccharide phosphate	260.0297	H+	C00092
1,2,3	251	17	Isoprenoid pathway	(R)-5-Phosphomevalonate	228.0399	Na+	C01107
1,2,3,4	190	341	Phosphonate	Demethylphosphinothricin	167.0347	Na+	C17962
1,2,3,4	441.3	310	Lipid	Hydroxycholesterol	402.3498	K+	C05500
1,2,3,4	639.2	414	Heme biosynthesis	Haem	616.1773	Na+	C00032
1,2,3,4	212.9	479	Chlorocyclohexane and chlorobenzene degradation	Chlorodienelactone	173.972	Ka+	C04706
1,2,4	109	479	Quinone	p-Benzoquinone	108.0211	H+	C00472
1,2,4	345.9	480	Amino acid metab	3-Iodo-L-tyrosine	306.9705	K+	C02515
1,3,4	169	19	Central metabolism	2-Oxoglutarate	146.0215	Na+	C00026
				2-Oxoisocaproate	130.063	K+	C00233
				3-Methyl-2-oxopentanoate	130.063	K+	C00671
				2-Dehydropantoate	146.0579	K+	C00966
				3-Phosphonopyruvate	167.9824	H+	C02798
				Phosphoenolpyruvate	167.9824	H+	C00074
2	313.2	287	Lipid	HPODE	312.2301	H+	C04717
2,3,4	519.1	400	Peptide	Nitro-hydroxy-glutathionyl-dihydronaphthalene	496.1264	Na+	C14803
2,4	71.1	373	Amino acid	Aminopropiononitrile	70.0531	H+	C05670
3	405.1	236	Isoprenoid pathway	Farnesyl diphosphate	382.131	Na+	C00448

Table S4. The metabolite IDs and candidate identification for the metabolites of interest from the unlabelled metabolic analyses. Related to Figure 3 and S2.

These metabolites were therefore upregulated in either one of the strains or in one of the light conditions. This table includes both the *Chlorella* and *P. bursaria* results.

Fraction	Upregulated in	Condition	Detected Mass	Retention Time	FDR	Pathway	Candidate Compounds	Exact Mass	Adduct	Kegg / Metacyc
Chlorella	HA1 strain	H & L light	247.2	336	*,**	Alkaloid/quinone	Anapheline	224.1889	Na+	C06183
							Geranylhydroquinone	246.162	H+	C10793
			283.3	336	*,**	Fatty acid	Oleate	282.2559	H+	C00712
		H light	218.2	17	*	Amino acid	L-Glutamylputrescine	217.1426	H+	C15699
							Alanyl-L-lysine	217.1426	H+	C05341
			265.3	337	*	Fatty acid	1-Hexadecanol	242.261	Na+	C00823
			385.2	375	*	Plant Hormone	Gibberellin A36	362.1729	Na+	C11862
			571.5	435	*	Carotenoid	Methoxyneurosporene	570.4801	H+	C15895
			589.4	420	*	Carotenoid	Echinenone	550.4175	K+	C08592
							Anhydrorhodovibrin	566.4488	Na+	C15877
							Hydroxychlorobactene	550.4175	K+	C15911
							3-Hydroxyechinenone	566.4124	Na+	C15966
	Low Light	HA1 strain	591.4	420	*	Carotenoid	Zeaxanthin	568.428	Na+	C06098
							Zeinoxanthin	552.4331	K+	C08590
							beta-Cryptoxanthin	552.4331	K+	C08591
							Xanthophyll	568.428	Na+	C08601
186 Strain	H & L light		743.5	373	*	Phosphoglyceride	1-18:3-2-trans-16:1-phosphatidylglycerol	742.4785	H+	CPD-2186
			105	15	*,**	Central metabolism	Hydroxypyruvate	104.011	H+	C00168
							Allophanate	104.0222	H+	C01010
			169	17	**	Central metabolism	2-Oxoglutarate	146.0215	Na+	C00026
							Phosphoenolpyruvate	167.9824	H+	C00074
							3-Phosphonopyruvate	167.9824	H+	C02798
							2-Oxoisocaproate	130.063	K+	C00233
							3-Methyl-2-oxopentanoate	130.063	K+	C00671
							2-Dehydropantoate	146.0579	Na+	C00966
							Coumarin	146.0368	Na+	C05851
			273.2	395	**	Fatty Acid	16-Hydroxypalmitate	272.2351	H+	C18218
			289.3	244	**	Diterpenoid	Kaurenol	288.2453	H+	C11872

Table S4 continued

Fraction	Upregulated in	Condition	Detected Mass	Retention time	FDR	Pathway	Candidate Compounds	Exact mass	Adduct	KEGG
Chlorella			337.3	380	**	Fatty acids	13;16-Docosadienoic acid	336.3028	H+	C16533
			607.3	361	**	Chlorophyll	Protoporphyrinogen IX	568.305	K+	C01079
			781.6	471	**	Ubiquinone	3-methoxy-4-hydroxy-5-nonaprenylbenzoate	780.2	H+	CPD-9898
			925.6	359	**	Chlorophyll	Bacterio-pheophytins	888.5765	K+	C05798
		H light	262.1	248	**	Folate	Dihydrobiopterin	239.1018	Na+	C00268
							6-Lactoyl-5;6;7;8-tetrahydropterin	239.1018	Na+	C04244
			323.2	248	*	Photoreception	Vitamin A aldehyde	284.214	K+	C00376
			335.3	372	**	Isoprenoids	Phytol	296.3079	K+	C01389
		L light	751.5	366	**	Ubiquinone	Octaprenyl-methyl-hydroxy-methoxy-1;4-benzoquinone	712.5431	K+	C05815
			273.3	268	**	Diterpenoid	Ent-Kaurene	272.2504	H+	C06090
P. bursaria 186 strain		H & L light	124	238	**, *	Vitamins and Cofactors	Niacin	123.032	H+	C00253
			126	217	**, *	Sulfur metabolism	Taurine	125.0147	H+	C00245
			170	237	**, *	Amino acid	Glutamate	147.0532	Na+	C00025
							5-Amino-4-oxopentanoate	131.0582	K+	C00430
							Glutamate 5-semialdehyde	131.0582	K+	C01165
			364.2	236	*, *	Antibiotic ?	ACV	363.1464	H+	C05556
		H light	396.1	237	*, *	Antibiotic ?	Deacetylcephalosporin C	373.0944	Na+	C03112
							Novobiocic acid	395.1369	H+	C12474
			352.2	237	*	Plant hormone?	trans-Zeatin riboside	351.1543	H+	C16431
			390.1	237	*	Amino/nucleotide sugar	N-Acetylneuraminate 9-phosphate	389.0723	H+	C06241
			416.1	250	**	Antibiotic ?	Cephalosporin C	415.1049	H+	C00916
							Chlorobiocic acid	415.0823	H+	C12471
		L light	434.1	249	*	Antibiotic ?	Novobiocic acid	395.1369	K+	C12474
			418.2	268	*	Sphingolipid	Sphingosine 1-phosphate	379.2488	K+	C06124



[Click here to access/download](#)

Supplemental Videos and Spreadsheets
Data S1.xlsx

